

Multimediator models for the galactic center gamma ray excess

James M. Cline and Grace Dupuis

Department of Physics, McGill University, 3600 Rue University, Montréal, Québec, Canada H3A 2T8

Zuwei Liu

Center for High Energy Physics, Tsinghua University, Beijing, 100084, China

Wei Xue

Center for Theoretical Physics, Massachusetts Institute of Technology, Cambridge, MA 02139, USA

Tentative evidence for excess GeV-scale gamma rays from the galactic center has been corroborated by several groups, including the Fermi collaboration, on whose data the observation is based. Dark matter annihilation into standard model particles has been shown to give a good fit to the signal for a variety of final state particles, but generic models are inconsistent with constraints from direct detection. Models where the dark matter annihilates to mediators that subsequently decay are less constrained. We perform global fits of such models to recent data, allowing branching fractions to all possible fermionic final states to vary. The best fit models, including constraints from the AMS-02 experiment (and also antiproton ratio), require branching primarily to muons, with a $\sim 10 - 20\%$ admixture of b quarks, and no other species. This suggests models in which there are two scalar mediators that mix with the Higgs, and have masses consistent with such a decay pattern. The scalar that decays to $\mu^+\mu^-$ must therefore be lighter than $2m_\tau \cong 3.6$ GeV. Such a small mass can cause Sommerfeld enhancement, which is useful to explain why the best-fit annihilation cross section is larger than the value needed for a thermal relic density. For light mediator masses ($0.2 - 2$) GeV, it can also naturally lead to elastic DM self-interactions at the right level for addressing discrepancies in small structure formation as predicted by collisionless cold dark matter.

1. INTRODUCTION

Indirect detection may offer the best hope of discovering the nature of dark matter beyond its generic gravitational effects. Currently there is a strong hint from Fermi Large Area Telescope data of dark matter annihilation in the galactic center (GC), giving rise to an excess of gamma rays peaking at energies of several GeV [1–6]. The morphology is consistent with that expected from dark matter annihilations, and the required cross section is of the right order of magnitude for yielding the correct thermal relic density. Millisecond pulsars are the main conventional astrophysical explanation that has been proposed [7–11] (see however refs. [12, 13] for alternative explanations). Arguments against the pulsar explanation have been given in refs. [14–16]. While the debate continues, the dark matter explanation remains a possibility that is still being widely explored [17]–[65].

The simplest models have heavy s -channel mediators leading to annihilations $\chi\chi \rightarrow f\bar{f}$ where f represents standard model particles that lead to gamma rays through their decays (or possibly inverse Compton scattering). However even if the mediator does not couple directly to light quarks, its coupling to any charged particle induces mixing with the photon at one loop, leading to dark matter scattering on nucleons. In many cases the induced coupling exceeds that allowed by direct detection searches, when the annihilation cross section for $\chi\chi \rightarrow f\bar{f}$ is large enough to explain the GC gamma-ray excess. Cosmic ray antiproton data also put pressure on direct annihilation to $b\bar{b}$ [66, 67] (see however [70]).

To escape direct detection and antiproton constraints,

one can consider the possibility of heavy mediators ϕ that are produced on shell in the annihilations $\chi\chi \rightarrow \phi\phi$, and subsequently decay. Even relatively slow decays due to very small couplings of ϕ to standard model particles can be consistent with the morphology of the GC signal, while making the models compatible with direct searches [68]–[81].

In the present study we reconsider light mediator models, motivated by new data sets for the GC excess, one from ref. [6] (hereafter CCW) and the other presented by the Fermi collaboration itself [83]. These results allow for heavier dark matter producing gamma rays up to higher energies ~ 100 GeV than the earlier determinations of [3, 4] which preferred lighter ~ 30 GeV dark matter, though the error bars are large enough for overlap of the allowed parameters. In addition we take into account constraints on annihilations producing electrons, from the AMS-02 experiment [84, 85]. These turn out to strongly disfavor direct annihilations into electrons that would produce a bump-like feature in the electron spectrum.

We find that the CCW and Fermi data show a strong preference for annihilation into mediators that decay with branching fractions $\sim 80 - 90\%$ to muons and $\sim 10 - 20\%$ to b -quarks. From a theoretical model building perspective this at first looks peculiar; for a single mediator to have such couplings is not suggested by any symmetry principle. On the other hand, singlet scalars that mix with the Higgs boson will decay preferentially into the heaviest possible standard model particle, since the couplings are just proportional to those of the Higgs. Therefore a more natural explanation is to have two me-

diators, one whose mass is between $2m_\mu$ and $2m_\tau$, and the other with mass between $2m_b$ and $2m_t$. (For a mediator with mass greater than $2m_h$ one must also consider decays into Higgs bosons.) By this combination of fitting to data and theoretical motivations, we are led to consider models with two scalar mediators with a hierarchy of masses. Remarkably, the best fit to the data puts the mediator masses in the ranges described above, which need not have been the case. This provides further experimental motivation for building models with several mediators, which at first might have seemed like a large theoretical leap.

We begin our analysis with an agnostic view concerning theoretical models, assuming only a single mediator for simplicity, and allowing for arbitrary branching ratios into different lepton and quark flavors, whose spectra are provided by ref. [86] (hereafter PPPC). We describe the construction of the χ^2 functions for fitting to the CCW and Fermi data, respectively, combined with those of AMS-02. The preference for final states consisting of an admixture of muons and b quarks is thereby established. We then focus on these final states, adding a separate mediator coupled to each one, and refit to the data. In the following section, a simple model of two scalars mixing with the Higgs is presented. We subsequently check whether the preferred models are consistent with

complementary constraints from direct detection, thermal relic density, cosmic microwave background, dwarf satellite observations, the antiproton flux ratio, and dark matter self-interactions. A simple two-mediator model is constructed that can fit the observations without excessive fine-tuning; Sommerfeld enhancement of the annihilation in the galaxy plays an important role. The model is shown to be consistent with LHC constraints on extra scalars mixing with the Higgs boson.

2. PREDICTED SIGNAL

The photon flux ($\text{GeV}/\text{cm}^2/\text{s}/\text{sr}$) from annihilation of Majorana DM particles in a given region around the GC can be expressed as

$$E_\gamma^2 \frac{dN^{\text{th}}}{dE_\gamma}(E_\gamma) = \frac{1}{2} \cdot \frac{\bar{J}\langle\sigma v\rangle}{4\pi m_\chi^2} \sum_f \text{BR}_{\phi \rightarrow f\bar{f}} E_\gamma^2 \frac{dN^f}{dE_\gamma} \quad (1)$$

where $\langle\sigma v\rangle$ is the averaged cross section for DM annihilation into two mediators, $\text{BR}_{\phi \rightarrow f\bar{f}}$ is the branching ratio for decays of the mediator ϕ into $f\bar{f}$ final states, and \bar{J} is the averaged J factor for the region of interest (ROI),

$$\bar{J} = \frac{\int_{\text{ROI}} d\Omega J(l, b)}{\int_{\text{ROI}} d\Omega} = \frac{\int_{\text{ROI}} \cos(b) db d\ell \int_0^\infty dx \rho^2 \left(\sqrt{x^2 + R_\odot^2} - 2xR_\odot \cos(\ell) \cos(b) \right)}{\int_{\text{ROI}} \cos(b) db d\ell} \quad (2)$$

For Dirac DM, one should replace the prefactor $1/2 \rightarrow 1/4$ in eq. (1), resulting in a cross section that is twice as large as that for Majorana DM, for a fixed observed flux. Unless otherwise stated we will assume Majorana DM in the following. The J factor depends upon the assumed shape of the DM density profile, which is commonly taken to be of the generalized NFW type,

$$\rho(r) = \rho_s \frac{(r/r_s)^{-\gamma}}{(1 + r/r_s)^{3-\gamma}} \quad (3)$$

Here we take $r_s = 20$ kpc and ρ_s such that $\rho_\odot = 0.4$ GeV/cm^3 in the solar neighborhood, with $R_\odot = 8.5$ kpc. Ref. [4] finds that the morphology of the GC excess is best fit by taking $\gamma = 1.26$, while ref. [6] adopts $\gamma = 1.2$.

dN^f/dE_γ is the photon spectrum from a single DM annihilation into $f\bar{f}$ final states, and comes from boosting the spectrum due to decay of the mediators ϕ [52]:

$$\frac{dN^f}{dE_\gamma} = \frac{2}{(x_+ - x_-)} \int_{E_\gamma x_-}^{E_\gamma x_+} \frac{dE'_\gamma}{E'_\gamma} \frac{dN_0^f}{dE'_\gamma} \quad (4)$$

where dN_0^f/dE'_γ is the photon spectrum from $\phi \rightarrow f\bar{f}$ in the rest frame of ϕ and $x_\pm = m_\chi/m_\phi \pm \sqrt{(m_\chi/m_\phi)^2 - 1}$.

For most final states, a Monte Carlo generator is needed to predict the distribution of photons from hadronization and decays. We take the spectra dN_0^f/dE from PPPC (ref. [86]), which is valid for mediator masses down to 10 GeV. For lighter mediators, extrapolation of the PPPC results would be required, introducing inaccuracies into the predictions. However our subsequent fits will dictate the need only for lighter mediators decaying into muons, for which we use an analytic expression for dN_0^μ/dE_γ [87], given in appendix B. The factor of 2 in (4) accounts for the two mediators produced in the annihilation.

3. DATA SETS

We consider three data sets for the GC excess: those of CCW [6], Fermi [83], and Daylan *et al.* [4]. Detailed descriptions follow; the data are summarized in fig. 1. We further include the AMS-02 measurement of the spectrum of cosmic ray electrons/positrons, and antiproton ratio data from the BESS, CAPRICE and PAMELA experiments. The antiproton data is not included in our

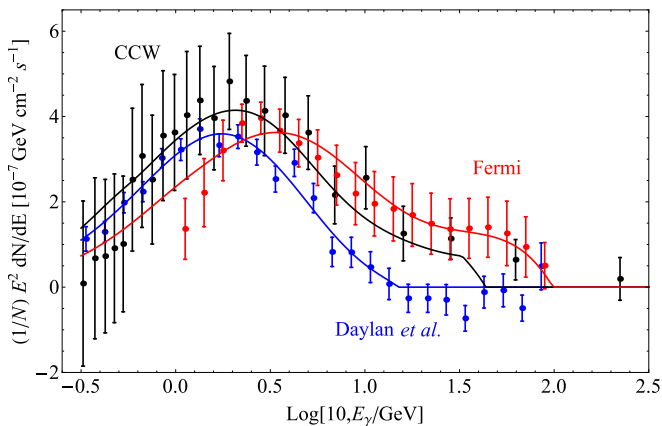


Figure 1: The three data sets for the GC gamma ray excess. The Fermi flux presented is the total flux from the $15^\circ \times 15^\circ$ square around the GC; the other two fluxes are normalised accordingly with same DM profile. Error bars for CCW are taken from the diagonal components of their covariance matrix. Solid curves are the predictions of the best-fit models described in section 4.

overall χ^2 function; rather we will verify after fitting the data that our models are compatible with the antiproton constraints.

3.1. CCW spectrum

The CCW spectrum (ref. [6]) is downloadable from [88], where a covariance matrix Σ for computing the χ^2 for fits to the data is also provided. Then

$$\chi^2 = \sum_{ij}^{24} \left(E_i^2 \frac{dN^{\text{th}}}{dE}(E_i) - E_i^2 \frac{dN^{\text{exp}}}{dE}(E_i) \right) (\Sigma^{-1})_{ij} \cdot \left(E_j^2 \frac{dN^{\text{th}}}{dE}(E_j) - E_j^2 \frac{dN^{\text{exp}}}{dE}(E_j) \right) \quad (5)$$

where the sum is over 24 energy bins, and $(\Sigma^{-1})_{ij}$ are the matrix elements of the inverse of the covariance matrix, obtained from columns 29-52 of the data file from [88]). This accounts for the correlations between the different energy bins.

The ROI for CCW is a $\pm 20^\circ$ square around the GC; in galactic coordinates, where ℓ is the longitude and b is the latitude, the region is

$$|\ell| < 20^\circ \text{ and } 2^\circ < |b| < 20^\circ \quad (6)$$

where the $\pm 2^\circ$ region in latitude is masked out to remove the galactic disk.

With these inputs and $\gamma = 1.2$ for the generalized NFW distribution, the J factor in (1) is $\bar{J} = 2.062 \times 10^{23} \text{ GeV}^2 \text{ cm}^{-5}$ for the CCW data. (This number agrees with [52].)

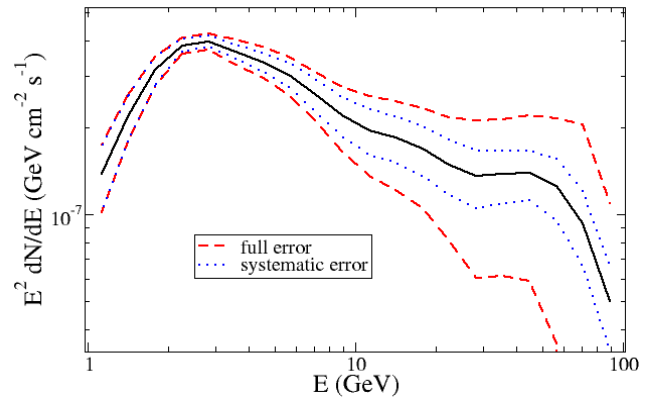


Figure 2: Spectrum for GeV excess from Fermi data, extracted from ref. [83]

3.2. Fermi spectrum

The Fermi collaboration has not officially released its data, but we have digitized it from the presentation in ref. [83], and list the results in table III, appendix A. Fluxes are given in 20 energy bins, equally spaced in $\log_{10}(E)$ between 1 MeV and 89 GeV. We estimate the statistical errors from taking \sqrt{N} for the number of total events in each bin and applying this to the part of the signal interpreted as the excess. Ref. [83] gives two characterizations of the spectrum of excess events, one which is presumed to be a power law in energy with an exponential cutoff, and the other being a separate fit to the excess in each bin. We adopt the latter for our analysis.

In addition to the statistical errors, there is systematic uncertainty associated with assumptions about the templates for background photons from pulsars and OB stars. We define the signal as the median between the upper and lower envelopes found from varying these templates, and the systematic error as the difference. This is added in quadrature with the statistical error to estimate the total uncertainty. The result is plotted in fig. 2, showing that errors are systematics-dominated at low energy, but mostly statistical at high energy. The χ^2 function is then defined in the usual way.

The ROI for the Fermi data is a $15^\circ \times 15^\circ$ square around the GC. Numerically integrating (2) we obtain $J = 1.07 \times 10^{23} \text{ GeV}^2/\text{cm}^5$, again assuming generalized NFW parameter $\gamma = 1.2$ and $\rho_\odot = 0.4 \text{ GeV}/\text{cm}^3$. Here we do not average over the solid angle (giving J instead of \bar{J}) because the Fermi data are reported as a total flux rather than an intensity flux.

3.3. Daylan et al. spectrum

Although our primary purpose is to explore the implications of the first two data sets which are more recent, for completeness we also apply our methodology to the GC excess spectrum determined in ref. [4]. It can be read

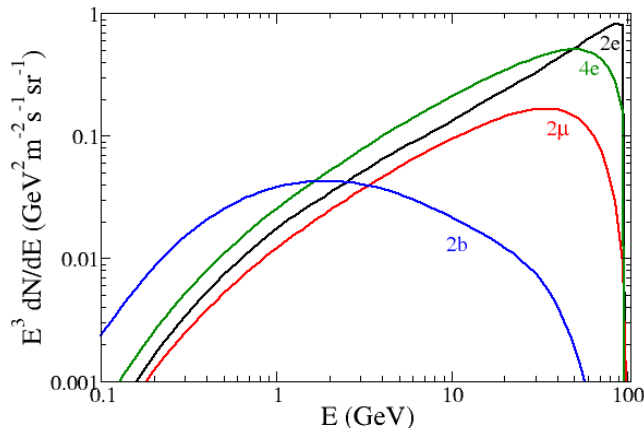


Figure 3: Electron spectra from dark matter annihilation into $2e$, $4e$, 2μ and $2b$, showing why annihilations directly into electrons are most strongly constrained by AMS-02 data.

from fig. 5 of that paper, from which it is straightforward to define χ^2 for a given predicted flux. The spectrum shown there has been normalized to correspond to a J factor that is not averaged over any solid angle, but instead is defined along a line of sight 5° away from the GC. For $\gamma = 1.2$, we thus find $J = 9.09 \times 10^{23} \text{ GeV}^2/\text{cm}^5$ (again using $\rho_\odot = 0.4 \text{ GeV}/\text{cm}^3$).

3.4. AMS positron/electron spectrum

AMS-02 published their recent results on the measurement of the e^+/e^- ratio and the separate electron and positron fluxes in [84, 85], confirming a positron excess above the expectations from standard cosmic ray propagation scenarios that was previously seen by PAMELA and Fermi. The more precise measurements of AMS-02 do not tell us whether the excess of the positron flux originates from dark matter or pulsars, but the smooth spectrum up to $\mathcal{O}(100)$ GeV already puts strong constraints on dark matter models [79, 89–91]. If light dark matter annihilates directly into e^+e^- , even though the spectrum is initially a delta function of energy, after propagation it leads to bump-like feature in the observed spectra. The feature is more spread out in models with decays into mediators, $\chi\chi \rightarrow \phi\phi \rightarrow 4e$, where the initial spectrum is box-like; nevertheless the final shape is still localized in energy and can be strongly constrained. The differences in shape of the electron spectra for relevant final states are illustrated in fig. 3.

To simplify our analysis and to make the results more model-independent, we assume that only dark matter annihilating to e^+e^- or $2e^+2e^-$ can be constrained by current AMS-02 data, since these have harder and more localized spectra compared to other channels. The latter also generate positrons and electrons, but they come from three- or four-body final states, which make the spectrum much softer and more broad. It would be easy to absorb

such nondistinctive contributions into the smooth background.¹ Following [79], we use polynomial functions to fit the logarithm of AMS spectra as the background. To obtain the electron/positron flux from light dark matter, a cosmic ray propagation model is chosen with a relatively large magnetic field, in order to achieve conservative bounds, since the energy loss is essentially due to the magnetic field and will soften the spectra.

Before including the light dark matter contribution, the absolute χ^2 of the background to fit against the AMS positron ratio data is $\chi^2 = 35.06$. This value does not depend on assumptions about the propagation model or solar modulations since we use fitting functions, rather than considering specific propagation models. However for the dark matter signal, the propagation and solar modulation uncertainties have to be considered. We marginalize over the range of the effective potential of solar modulation, $[0, 1 \text{ GV}]$ and a relatively large magnetic field is chosen to propagate positrons and electrons from dark matter annihilation.² The 3σ exclusion curves for dark matter annihilating to $2e^+2e^-$ are illustrated in fig. 5 for two different mass ratios m_ϕ/m_χ . The strong constraints from AMS lead us to models with negligible direct annihilations into electrons.

3.5. Antiproton ratio

The current measurements of the cosmic ray antiproton flux agree well with the expected astrophysical backgrounds; therefore, they are able to significantly constrain the cross section for dark matter annihilation to hadronic final states, modulo the uncertainties from cosmic ray propagation. Following [93], we use antiproton ratio data from the BESS [94, 95], CAPRICE [96] and PAMELA [97] experiments. In order to minimize the systematic uncertainties from different experiments, the antiproton ratio data are employed here, rather than the antiproton flux data. Parameters governing cosmic ray propagation are constrained by fitting to the observed ratio of boron to carbon, but this still leaves some freedom to vary parameters, as well as the solar modulation; this leads to a range of estimates for the astrophysical background of proton and antiproton fluxes, that are consistent with the observed fluxes from the above data sets. Once the propagation model, the solar modulation and the astrophysical background are fixed, we can perform a χ^2 fit of the \bar{p}/p data by adding the contribution from the dark matter annihilation.

¹ The background may include contributions from primary and secondary electrons, secondary positrons, pulsars, or heavy dark matter annihilation/decay. All of them could contribute to the smooth spectra observed by AMS-02.

² The total magnetic field is composed of a regular one and a turbulent one. We normalize the total value at the Sun to $B_\odot = 15\mu\text{G}$.

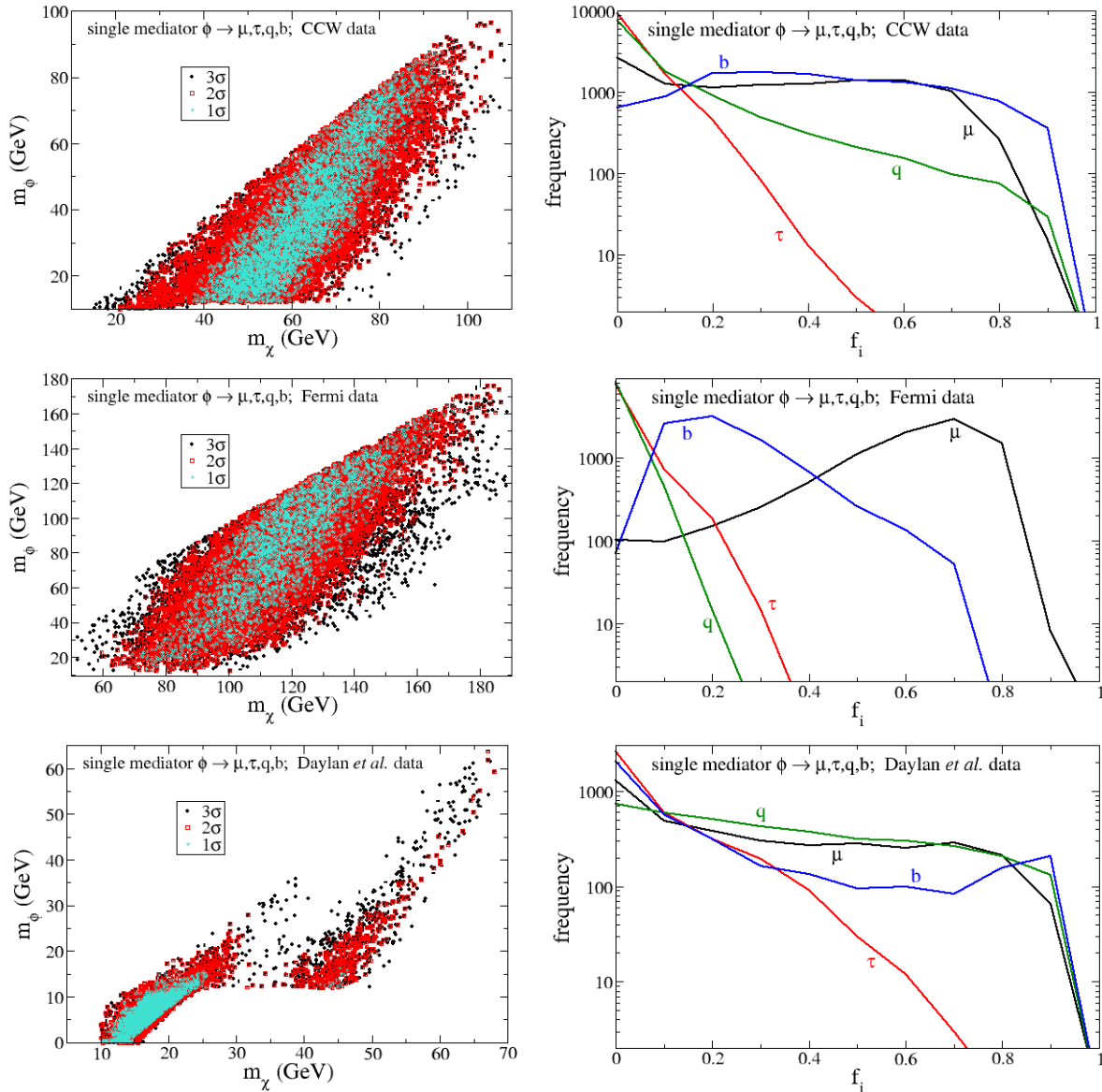


Figure 4: Left column: distribution of m_ϕ versus m_χ for single-mediator models from fitting to CCW, Fermi and Daylan *et al.* data (from top to bottom), with $f_e = 0$ and floating branching fractions to μ, τ, q, b . Right column: corresponding distributions of f_μ, f_τ, f_q, f_b .

Two benchmark propagation models are used here to cover the systematic uncertainties of the cosmic ray propagation: KRA and THN, in the notation of ref. [92], where the main difference of the two models is the halo height, with $z_t = 4$ kpc for KRA, and $z_t = 0.5$ kpc for THN. The other parameters are the slope of the diffusion coefficient $\delta = 0.5$, nuclei spectral index $\gamma = 2.35$, the normalization of the diffusion coefficient $D_0 = 2.68 \times 10^{28} \text{ cm}^2 \text{ s}^{-1}$, and the solar modulation potential $\Phi = 0.95$ GV for the KRA model. For THN these take the same values except for $D_0 = 0.32 \times 10^{28} \text{ cm}^2 \text{ s}^{-1}$. Neither of these models consider convection. Further details can be found in [93].

The resulting antiproton constraints on DM annihilat-

ing to $b\bar{b}b\bar{b}$ with two different ratios of mediator mass to DM mass are shown in fig. 6. The dependence on propagation model is the largest uncertainty, with THN (dashed lines) giving a factor of 10 weaker constraints than KRA (solid lines), while the dependence on the mediator mass is relatively weak (red versus blue curves). We adopt the more conservative bounds from the THN model in our analysis. It will turn out that in our preferred models with a subdominant branching fraction to b quarks, the antiproton limit is not significantly constraining (see fig. 9 below).

Better measurements of heavy nuclei abundances from AMS-02, in particular the boron/carbon ratio, may improve our understanding of cosmic ray propagation mod-

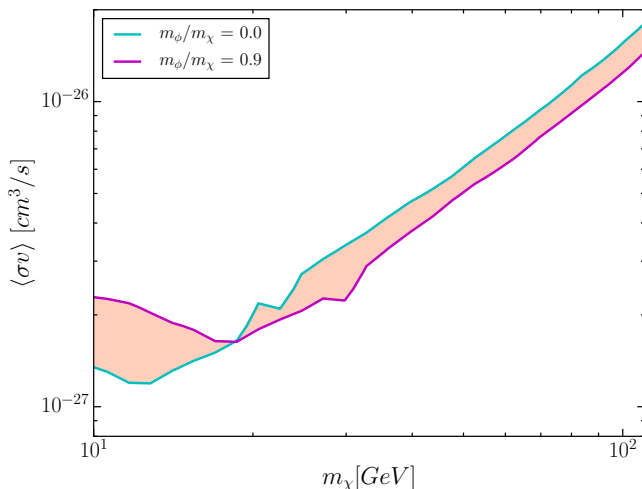


Figure 5: AMS exclusion curves for $\chi + \chi \rightarrow 2\phi \rightarrow 4e$. The exclusion limit for two values of $m_\phi/m_\chi = 0$ and 0.9 are shown here, to illustrate the (relatively weak) dependence on the mediator mass.

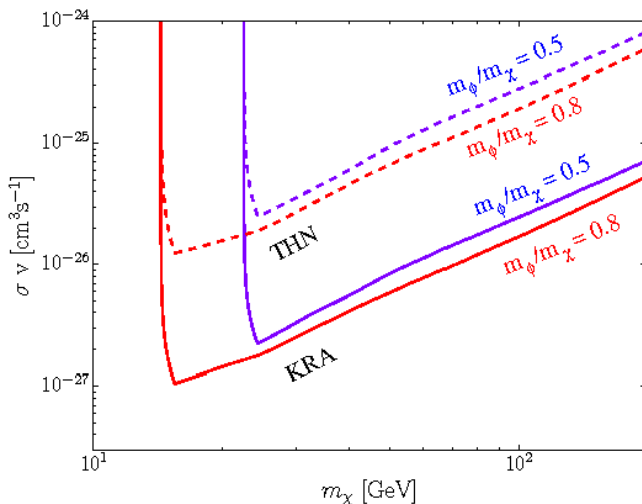


Figure 6: Antiproton exclusion curves for $\chi + \chi \rightarrow 2\phi \rightarrow b\bar{b}b\bar{b}$. The 3σ exclusion limit for two propagation models, KRA and THN, and for two values of $m_\phi/m_\chi = 0.5$ and 0.8 are shown here respectively.

els, hopefully leading to a decrease in the systematic uncertainty from the propagation models. Moreover a much more precise measurement of antiproton data itself is expected to improve this limit by a factor of two or three. Considering both effects, we anticipate that coming AMS-02 data may shed further light on which DM models can consistently explain the GC excess.

4. FITS WITH A SINGLE MEDIATOR

Our initial motivation was to reexamine the viability of kinetically mixed Z' models for the GC excess in light

Data set	m_χ	m_ϕ	f_μ	f_τ	f_q	f_b	$\langle\sigma v\rangle$	χ^2_{\min}	DOF
CCW	46	12.3	0.82	0	0.02	0.16	1.1	18.8	24
Fermi	130	114.5	0.80	0	0	0.20	2.8	6.4	20
Ref. [4]	14.6	4.0	0.49	0.01	0.06	0.44	0.7	22.9	25

Table I: Best fit parameters for single-mediator model fits to the three data sets. Masses are in GeV units, $\langle\sigma v\rangle$ in units of $10^{-25} \text{ cm}^3/\text{s}$. “DOF” is the number of data points in each set.

Data set	m_χ	m_ϕ	χ^2_{\min}	Data set	m_χ	m_ϕ	$\langle\sigma v\rangle$	χ^2_{\min}
CCW (μ)	8.5	1	37	CCW (b)	75	37	0.6	23.6
Fermi (μ)	14	1	42	Fermi (b)	153	102	1.5	20.5
Ref. [4] (μ)	7.5	1	51	Ref. [4] (b)	51	25	0.4	27.5

Table II: Best fit parameters for single-mediator model fits to the three data sets, allowing for 100% branching to μ final states (left) or b (right). Masses are in GeV units, $\langle\sigma v\rangle$ in units of $10^{-25} \text{ cm}^3/\text{s}$.

of the new data sets from CCW and Fermi. Although a good fit to the GC excess can be obtained, these models necessarily have a significant branching fraction into electrons. We found that the combined fit to the GC excess and AMS electron data was quite poor.

This suggests doing a model-blind search for different combinations of final state fermions that could give a good fit to all data. We performed this in the 8-parameter space of models characterized by the DM and mediator masses m_χ , m_ϕ , and branching fractions f_i for annihilation into final states $i = e, \mu, \tau, q, c, b$, where q denotes light quarks, whose spectra are all provided by PPPC [86]. These fractions are subject to the constraint $\sum_i f_i = 1$, where we ignore invisible channels since this degree of freedom would be degenerate with the overall cross section $\langle\sigma v\rangle$, which makes the 8th parameter.

The result of this search is that f_e must be negligible as a result of the AMS constraint. Therefore for more refined searches we set $f_e = 0$ and remove the AMS contribution from the total χ^2 . We find that the CCW and Fermi GC spectra further disfavor any significant contribution from τ , q or c , preferring an admixture of muons and b quarks. We sample models with χ^2 near the minimum value using a Markov Chain Monte Carlo (MCMC) search as well as Multinest [99]; this prevents getting stuck in spurious local minima of the χ^2 function. In this way we find a large spread in allowed masses m_χ and m_ϕ as shown in fig. 7. The best fit values of parameters for the three data sets are listed in table I.

However the nominal best-fit values should not be given too much importance, because there are quasi-degeneracies in the χ^2 functions that allow for good fits to the data over a range of parameters for the Fermi and CCW data sets. These are illustrated in fig. 7. We see that m_χ can vary in the range 40-100 GeV keeping $\Delta\chi^2 \lesssim 2$ for the CCW fits. Similarly the Fermi data are compatible with m_χ in the range 80-180 GeV. Both

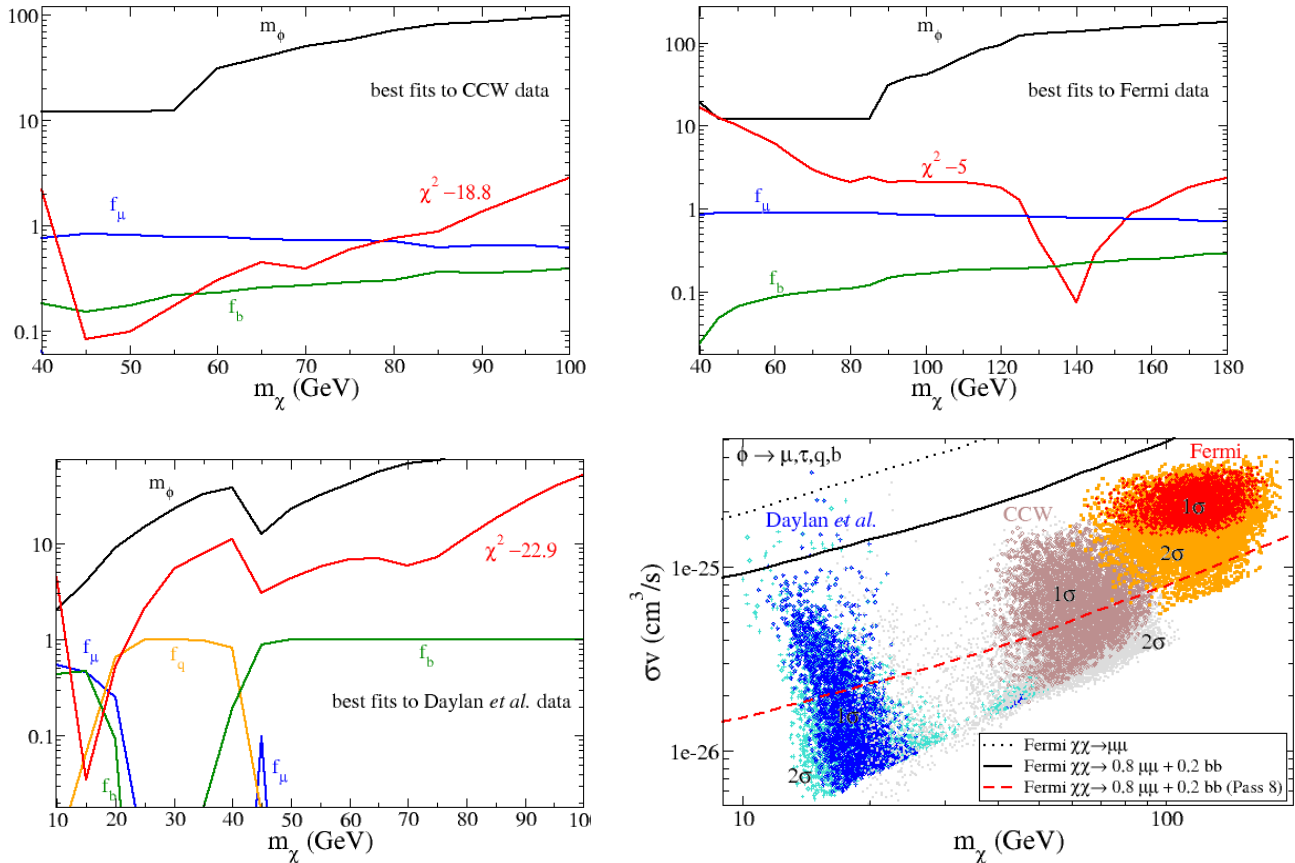


Figure 7: Top row and bottom left: best-fit values of m_ϕ (in GeV), f_μ and f_b as a function of m_χ for data from CCW (top left), Fermi (top right) and Daylan *et al.* (bottom left). Bottom right: distributions of cross sections versus m_χ (1-2 σ allowed regions) for the three data sets, compared to estimated Fermi limits from $\chi\chi$ annihilation to $\mu\mu + bb$ in dwarf satellites (see text).

data sets are compatible with annihilations into $\mu\bar{\mu}$ and $b\bar{b}$, with the former being dominant. The corresponding results for the Daylan *et al.* spectrum are qualitatively different, both for the lower range of m_χ and the final states, which prefer μ , q or b depending upon m_χ . A range of larger masses $m_\chi \sim 55 - 70$ GeV is however still reasonable with $\Delta\chi^2 \sim 6$. This provides overlap with the preferred regions of the other data sets.

The required values of the annihilation cross section $\langle\sigma v\rangle$ needed to fit the magnitude of the excess are illustrated in fig. 7 (bottom right). The 1-2 σ favored regions in the m_χ - $\langle\sigma v\rangle$ plane are somewhat disjoint between the three data sets. We show for comparison estimated limits on annihilation to 80% $\mu\mu + 20\% bb$ from Fermi observations of satellite galaxies of the Milky Way [100], with an interpolation to the case of interest for us of $f_\mu \sim 0.8$, $f_b \sim 0.2$ using $\langle\sigma v\rangle^{-1} \cong f_\mu\langle\sigma_\mu v\rangle^{-1} + f_b\langle\sigma_b v\rangle^{-1}$. Here the σ 's refer to the limiting values. This is a rough estimate of the expected limit on our best-fit models to the CCW and Fermi GC excess data, which is seen to be still consistent with most of the preferred parameter space. Also plotted is our estimate of the limit on $\langle\sigma_b v\rangle$ from Fermi's Pass 8 data [101], which is lower than that of ref. [100]

by a factor of 5. These results indicate some tension between the dwarf limits and the GC excess signal. This can be relieved somewhat, still consistently with our fits, by reducing the fraction f_b so that the signal is more μ -like. Fig. 7 (bottom right) shows that the constraints into pure μ final states are significantly weaker.

Since the allowed ranges for m_χ include values greater than m_W and m_Z , we have also performed Monte Carlo searches of the enlarged parameter space allowing for branching into W and Z . However we find that the best fit models have negligible branching into these states, and so we henceforth disregard them.

One may wonder whether the preference for an admixture of μ and b final states is statistically significant compared to 100% branching to either μ or b . We have scanned over m_χ and m_ϕ for these cases to compare with the previous results for admixtures of final states. The best-fit parameters and minimum values of χ^2 are given in table II, to be compared to the results of table I. Annihilations to μ only give poor fits to all data sets, while those to b do better. Nevertheless, the improvement from allowing an admixture of μ and b is statistically significant. The q and τ channels play a negligible role in the

fits to multiple final states, so these can be considered as approximately the same as having only mixed μ and b states. The improvements in χ^2 with two channels versus b only is 4–5 for the CCW and ref. [4] data sets, and 14 for the Fermi data. In all cases $\delta\chi^2 \gg 1$ for the inclusion of one extra parameter.

Physically, the preference for two final states arises because the spectrum from any one of them falls with energy as a power law times an exponential cutoff. Especially for the Fermi data (see fig. 1), the observed spectrum does not have this form but instead remains high to large energies, just before abruptly cutting off. The superposition of final state spectra from μ and b is able to reproduce this shape much better than that from bs alone.

5. FITS WITH TWO MEDIATORS; SOMMERFELD ENHANCEMENT

The previous analysis shows that annihilation to a mixture of b and μ final states gives the best fits to Fermi and CCW data. From a model-building point of view, it may seem ad-hoc to couple the mediator to the standard model fermions in this way. If the mediator is a singlet that mixes with the Higgs, the couplings are proportional to the masses of the fermions. With two such mediators however, the desired mixture of final states could be a natural consequence of the masses m_{ϕ_1} and m_{ϕ_2} , only requiring that $m_{\phi_1} < 2m_\tau$ and $2m_b < m_{\phi_2} < m_\chi$, so that decays into disfavored channels are kinematically forbidden, or suppressed by small Yukawa couplings. Motivated by this theoretical consideration and the previous results, we thus reconsider the data in the model with five parameters

$$\{m_\chi, m_{\phi_1}, m_{\phi_2}, f_b/f_\mu, \langle\sigma v\rangle\}$$

This is one fewer parameter than in the single-mediator models, where we had two additional final states.

Interestingly, the fits to Fermi and CCW data, in which m_{ϕ_1} is free to vary, are consistent with values that are not far from the theoretical threshold $2m_\tau$. In fig. 8 we plot best-fit parameters that are at least local minima of χ^2 , demonstrating this assertion. χ^2 is sufficiently flat as a function of m_{ϕ_1} that the models remain good fits even when m_{ϕ_1} is restricted to stay below $2m_\tau$, as is also shown in the figure. Monte Carlo searches of the parameter space reveal slightly better fits ($\delta\chi^2 \sim 0.1 - 0.2$) with higher m_{ϕ_1} , but these do not contradict the goodness of fit of the models with $m_{\phi_1} < 2m_\tau$.

Using MCMC to explore parameters in the model with m_{ϕ_1} fixed at 3 GeV, we find that the branching fraction to muons, f_μ , is concentrated near 0.9 for fits to Fermi, while having a broader distribution in CCW. This is shown in fig. 9(left). The best-fit values of the annihilation cross section $\langle\sigma v\rangle$ are shifted upwards by a factor of a few in these models relative to the single-mediator model, as can be seen from fig. 9(right) in comparison

to fig. 7 (bottom right). Here we also show constraints on annihilations from Fermi dwarf observations (see discussion of fig. 7), and from our analysis of antiproton constraints, for the representative case of 20% branching fraction to b quarks, except for the latest Pass 8 constraint, where we use 10% to b quarks. There is strong tension between this limit and the preferred region for the GC excess of the Fermi data, while some compatibility with the CCW data remains. The antiproton limit on the cross section is relaxed by a factor of 5 compared to the limit for annihilations purely into bs shown in fig. 6. The cross sections needed for the GeV excess are still comfortably below this limit (and more so in the single-mediator model where the target value of the cross section is lower).

5.1. Sommerfeld enhanced annihilation

The fact that these cross sections are significantly higher than the nominal value $\langle\sigma v\rangle_0 \equiv 3 \times 10^{-26} \text{cm}^3/s$, needed for approximately the right relic density, is potentially a cause for concern. Such large cross sections would significantly suppress the density of χ , in contradiction to our assumptions. However the presence of the light mediator ϕ_1 provides a possibility for resolving this problem, due to the low velocities of DM in the galaxy relative to the early universe, and the resulting nonperturbative Sommerfeld enhancement of the cross section by multiple exchanges of ϕ_1 .

Let us suppose that ϕ_1 couples to χ with strength g_1 and define $\alpha_1 = g_1^2/4\pi$. (Later we will see that both scalar g_1 and pseudoscalar $g_{1,5}$ couplings are needed to get s -wave annihilation, but that $g_{1,5} \ll g_1$.) The Sommerfeld enhancement S is controlled by the two small parameters [102]

$$\epsilon_\phi = \frac{m_{\phi_1}}{\alpha_1 m_\chi}, \quad \epsilon_v = \frac{v}{\alpha_1} \quad (7)$$

A good approximation to S is given by the expression [103, 104]

$$S = \left(\frac{\pi}{\epsilon_v}\right) \frac{\sinh X}{\cosh X - \cos \sqrt{(2\pi/\bar{\epsilon}_\phi) - X^2}} \quad (8)$$

where $\bar{\epsilon}_\phi = (\pi/12)\epsilon_\phi$ and $X = \epsilon_v/\bar{\epsilon}_\phi$. (The cosine becomes cosh if the square root becomes imaginary.)

To quantify the magnitude of Sommerfeld enhancement needed, and the corresponding coupling strengths α_1 , for each model in our MCMC chains we estimate the needed value of S as the actual cross section $\langle\sigma v\rangle$ divided by the nominal relic density value $\langle\sigma v\rangle_0$, assuming that $v = 10^{-3}$. Typically there are several coupling strengths that can yield the required value of S due to resonances, illustrated in fig. 10(left). Scanning over α_1 , we find the minimum value of the coupling needed to get the required enhancement. The distributions of S versus α_1 for fitting the Fermi and CCW data are shown in fig. 10(right). It

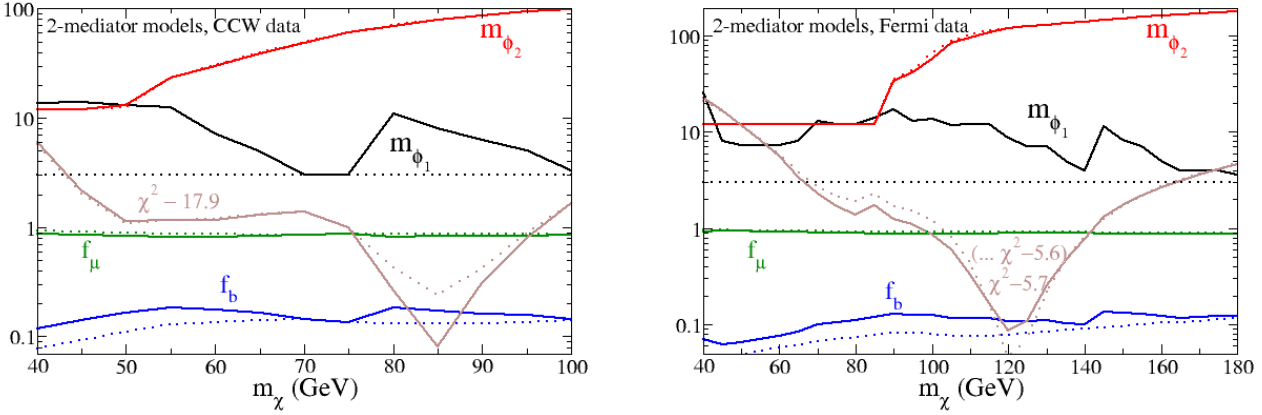


Figure 8: Left: best fits as a function of m_χ to the CCW data, as in fig. 7. Solid lines have m_{ϕ_1} freely varying, while dotted ones restrict $m_{\phi_1} = 3$ GeV. Right: same for Fermi data.

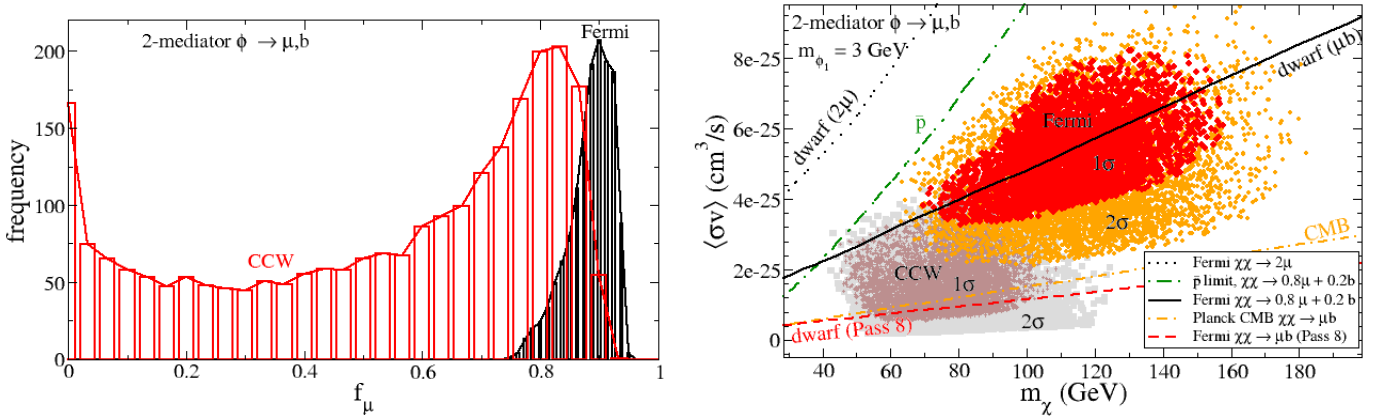


Figure 9: Left: distribution of branching fraction to muons for two-mediator model, with m_{ϕ_1} fixed at 3 GeV. Right: corresponding distributions of $\langle\sigma v\rangle$ versus m_χ , with Fermi dwarf galaxy constraints overlaid, as well as our constraint from antiprotons and that from the CMB.

is noteworthy that we can get the right amount of enhancement by invoking reasonably small values of the couplings, with $0.01 \lesssim \alpha_1 \lesssim 0.06$.

6. PARTICLE PHYSICS MODELS

To further explore the implications of dark matter with two scalar mediators, such as from the thermal relic density requirement and direct detection constraints, we need to more fully specify the interactions. We will allow for parity-breaking in the dark sector, with both scalar and pseudoscalar couplings

$$\mathcal{L}_{\text{int}} = \sum_{i=1}^2 \bar{\chi} \phi_i (g_i + i g_{i,5} \gamma_5) \chi \quad (9)$$

This choice is meaningful if the DM mass m_χ is restricted to be real; otherwise $g_{i,5}$ can be rotated away by a chiral redefinition $\chi \rightarrow e^{i\theta\gamma_5}\chi$. The ansatz (9) is motivated by

the fact that the cross section for $\chi\bar{\chi} \rightarrow \phi_i\phi_j$ is p -wave suppressed unless both types of couplings are present. For simplicity we take both mediators to be real fields.

However, both scalars are required to get VEVs in order to mix with the SM Higgs and hence couple to SM fermions, so in fact eq. (9) would lead to a complex m_χ once the VEVs are taken into account, and we would have to redefine the fields to make it real. Instead we will regard (9) as describing the low-energy effective theory where this has already been carried out.

The other important parameters of the model are the mixing angles θ_i between the mediators and the SM Higgs. These are determined by cross-couplings $\frac{1}{2}\lambda_i\phi_i^2|H|^2$ and VEVs,

$$2\theta_i \cong \frac{\lambda_i \langle\phi_i\rangle v}{m_h^2 - m_{\phi_i}^2} \quad (10)$$

in the limit of $\theta_i \ll 1$, where $v = \sqrt{2}\langle H\rangle = 246$ GeV. For our purposes, knowledge of the individual parameters λ_i and $\langle\phi_i\rangle$ is not necessary, and we will work directly with

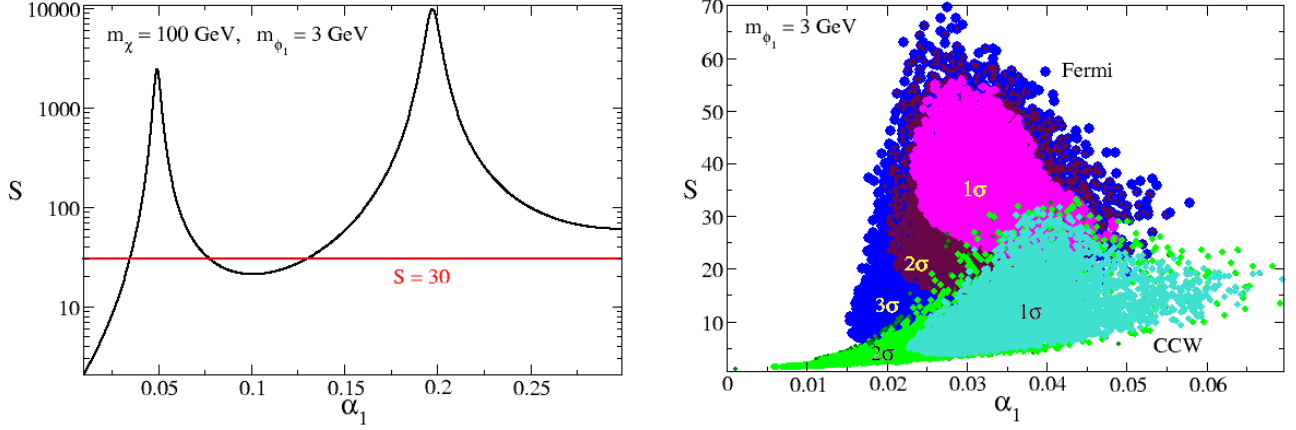


Figure 10: Left: example of Sommerfeld enhancement factor as a function of coupling $\alpha_1 = g_1^2/4\pi$ of light mediator ϕ_1 to dark matter, with $m_\chi = 100$ GeV and $m_{\phi_1} = 3$ GeV. Typical required value of $S = 30$ is shown by the horizontal line, for reference. Right: scatter plot of required values of S versus minimum value of α_1 corresponding to sample of models in fig. 9.

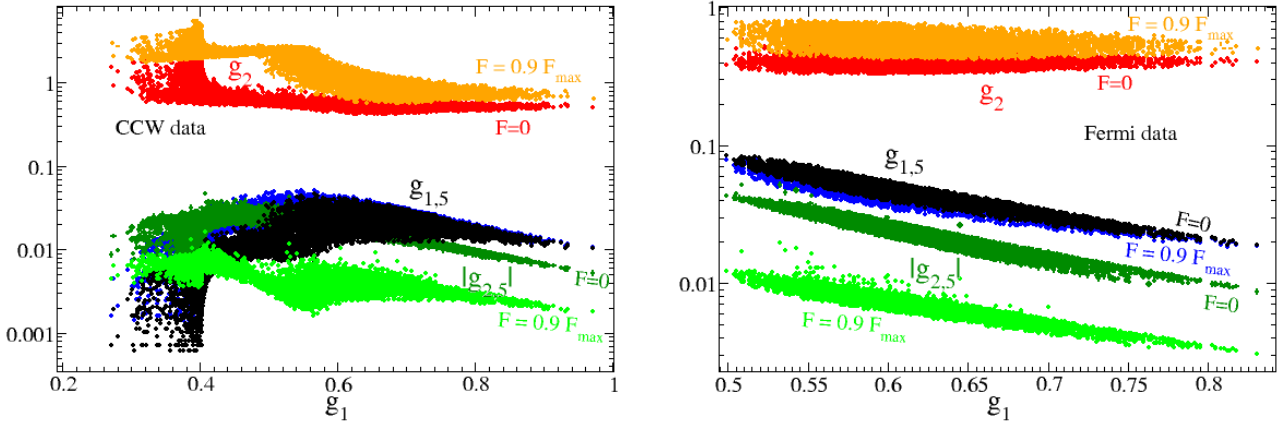


Figure 11: 2σ -allowed values of mediator couplings to DM for fits to CCW (left) and Fermi (right) data sets. Regions differ depending upon the choice a one free combination of couplings which we take to be F (eq. (14), which we illustrate for $F = 0$ and $F = 0.9 F_{\max}$ (see eq. (C4)).

the θ_i , that lead to couplings of the mediators to SM fermions ψ of the form

$$\theta_i y_j \phi_i \bar{\psi}_j \psi_j \quad (11)$$

where $y_j = m_j/v$ is the SM Yukawa coupling.

For simplicity we have neglected the mediator mixing mass $m_{12}^2 \phi_1 \phi_2$ and the cross-coupling $\lambda_{12} \phi_1^2 \phi_2^2/4$. They get generated at one loop by a virtual Higgs or χ , at the level $\lambda_{12} \sim (\lambda_1 \lambda_2 - g_1^2 g_2^2)/(16\pi^2)$. Cubic terms $\phi_1 \phi_2^2$ and $\phi_2 \phi_1^2$ can be forbidden by the discrete symmetry $\phi_i \rightarrow -\phi_i$, $\chi \rightarrow e^{i\pi\gamma_5/2} \chi$ as long as χ gets all of its mass from the singlet VEVs (in our case primarily $\langle \phi_2 \rangle$). This symmetry is spontaneously broken by the VEVs of ϕ_i so these terms get generated at one loop. They allow for the decay $\phi_2 \rightarrow \phi_1 \phi_1$ which we have ignored. Taking it into account will require some small shift in the values of g_1/g_2 needed to get the desired ratio of muons to b quarks for the GC excess signal, but since the data are

not yet good enough to determine these couplings precisely, we do not expect the $\phi_2 \rightarrow \phi_1 \phi_1$ decay channel to change our results significantly.

To see how much fine-tuning is required by our neglect of ϕ_1 - ϕ_2 mass mixing, the most important term to consider is the χ -loop diagram connecting ϕ_1 to ϕ_2 , and leading to $m_{12}^2 \sim g_1 g_2 m_\chi^2/(16\pi)$. If m_1^2 and m_2^2 denote the diagonal terms in the mass matrix, the lightest eigenvalue is given by

$$m_{\phi_1}^2 \cong m_1^2 - \frac{m_{12}^4}{m_2^2} \quad (12)$$

Taking $m_2 \sim m_\chi \sim 100$ GeV, the second term is of order -1 GeV², similar in size to m_1^2 (we have assumed $m_1 = 3$ GeV for our benchmark models). Therefore no extraordinary fine tuning seems to be required in our model to keep m_1 small (of course we ignored here the Planck-scale hierarchy problem and took the heaviest threshold

in the hidden sector for the estimate of the loop contribution). An accidental cancellation between the terms in (12) could even help to explain the smallness of m_1 .

7. RELIC DENSITY

The relic density of χ is determined by $\chi\bar{\chi} \rightarrow \phi_i\phi_j$ summed over all possible final states. At kinematic threshold we find that

$$\sigma v_{\text{rel}} \cong \sum_{i=1,2} \frac{g_i^2 g_{i,5}^2 m_\chi \sqrt{m_\chi^2 - m_i^2}}{8\pi (m_\chi^2 - m_i^2/2)^2} + \frac{F^2}{16\pi(m_\chi^2 - m_2^2/4)} \quad (13)$$

where for simplicity we approximated $m_1 = 0$ in the second line, and defined

$$F = (g_1 g_{2,5} + g_2 g_{1,5}) + (g_1 g_{2,5} - g_2 g_{1,5}) \frac{m_2^2}{4m_\chi^2} \quad (14)$$

The couplings are constrained by the fits to the GC excess indicating that the number of muons to b quarks produced in the annihilations is given by

$$\frac{N(\mu)}{N(b)} = \frac{N(\phi_1)}{N(\phi_2)} \sim \frac{(g_1 g_{1,5})^2 + F^2/4}{(g_2 g_{2,5})^2 + F^2/4} \quad (15)$$

For simplicity we here omitted the dependence upon m_2^2/m_χ^2 implied by eq. (13), but the more exact expression is given in appendix C (eq. (C2)).

By demanding that $\langle\sigma v\rangle$ matches the canonical cross section $\langle\sigma v\rangle_0 = 3 \times 10^{-26} \text{ cm}^3/\text{s}$ for approximately achieving the observed relic density, and also that (C2) gives the required ratio of μ/b for a given model realization, we get two constraints on the couplings. The requirement of sufficient Sommerfeld enhancement gives a third, fixing the magnitude of g_1 . We can take the value of F in (14) as a free parameter that can be varied to explore the range of possible solutions for $g_i, g_{i,5}$ characterizing viable models. Details of the algebraic solution for the couplings are given in appendix C.

We have carried out the above procedure for the models in our Monte Carlo searches that give good fits to the GC GeV excess, to find the ranges of allowed values for the couplings. Scatter plots of $g_{1,5}, g_2, g_{2,5}$ versus g_1 are shown in fig. 11 for fits to the Fermi and CCW data sets, within the 2σ -allowed regions. Here we have assumed solutions for g_i that give the smallest values of the couplings (since a quadratic equation must be solved leading to a second branch of solutions with larger values). Interestingly, the parity-conserving couplings turn out to be the largest, with $g_1 \sim g_2 \sim (0.5 - 0.8)$, while the parity-violating couplings are suppressed, with $g_{1,5} \sim (0.02 - 0.1)$ and $|g_{2,5}|$ being smaller. The exact range of $g_{2,5}$ (which we take to be negative, see appendix C) is the least constrained of all the couplings,

with $g_{2,5} = 0$ always being a possibility (corresponding to $F = F_{\text{max}}$), since we have freedom to impose this as an extra condition while satisfying the remaining physical constraints. But in no case can $|g_{2,5}|$ be large while maintaining that μ final states dominate over b for the GeV excess spectral shape.

8. DIRECT DETECTION

The cross section for scattering on nucleons (with mass m_p) is dominated by exchange of the light ϕ_1 mediator,

$$\sigma_p \cong \frac{(g_1 \theta_1 y m_p)^2}{\pi m_{\phi_1}^4} \quad (16)$$

in the limit that $m_\chi \gg m_p$. Direct detection limits put an upper bound on $g_1 \theta_1$ that depends upon m_χ as shown in fig. 12 for fixed $m_{\phi_1} = 3 \text{ GeV}$. Here y is the Higgs-nucleon coupling, which we take to be $y = 1.3 \times 10^{-3}$ (see ref. [105] for a recent review). For $m_\chi \sim 100 \text{ GeV}$ as suggested by our fits to the GC excess, this gives $g_1 \theta_1 < 2 \times 10^{-5}$. On the other hand the Sommerfeld enhancement determined in section 5.1 demands that $\bar{g} \sim 0.6$, so $\theta_1 \lesssim 3 \times 10^{-5}$. Eq. (10) then implies $\lambda_1 \langle\phi_1\rangle < 4 \times 10^{-3} \text{ GeV}$. We can eliminate the singlet VEV using its relation to the ϕ_1 mass and self-coupling $\bar{\lambda}_1$ by $m_{\phi_1} = \sqrt{2\bar{\lambda}_1} \langle\phi_1\rangle$. Taking $m_{\phi_1} = 3 \text{ GeV}$, we see that the direct detection constraint implies a hierarchy between the scalar quartic couplings,

$$\frac{\lambda_1}{\bar{\lambda}_1^{1/2}} < 2 \times 10^{-3} \quad (17)$$

This is not technically unnatural since the coupling λ_1 only receives multiplicative renormalizations.

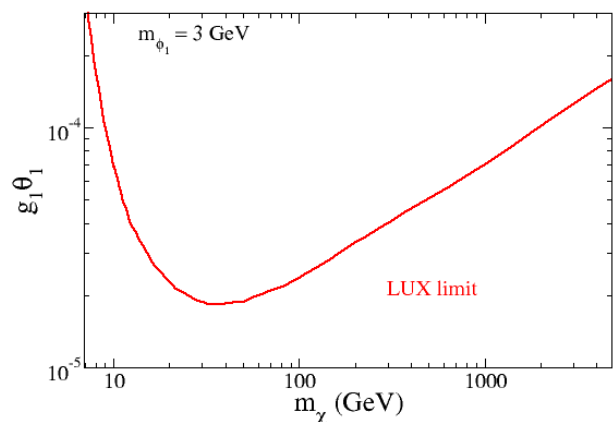


Figure 12: Upper limit on DM coupling times mixing angle of the light mediator ϕ_1 from LUX [106] direct search.

9. COSMOLOGICAL CONSTRAINTS

We consider here the impact of cosmic microwave background constraints, and those coming from scattering of dark matter on itself in this section. We will show that the models treated in this work are compatible with current data, but are close to the limits, with interesting potential to address puzzles in the small scale structure of galaxies predicted by noninteracting cold dark matter.

9.1. Cosmic microwave background

Dark matter annihilations into charged particles during the epoch of reionization can impact the temperature and polarization fluctuations of the cosmic microwave background (CMB) [107]-[112], leading to constraints on the annihilation cross section that are particularly strong for low DM masses, scaling linearly with m_χ . At this late era, the DM velocity is already sufficiently low that the magnitude of Sommerfeld enhancement occurring in collisions at the galactic center will be operative also for the CMB. Therefore we can directly compare the cross sections needed for the GC excess to the CMB limits.

The CMB limits are depend upon the efficiency f_{eff} for given final state particles to deposit energy electromagnetic energy in the plasma. The latest upper limit on the annihilation cross section using Planck temperature and polarization data can be expressed as

$$f_{\text{eff}} \langle \sigma v \rangle < 4 \times 10^{-26} \left(\frac{m_\chi}{100 \text{ GeV}} \right) \text{cm}^3/\text{s} \quad (18)$$

which we infer from fig. 41 of ref. [113]. Ref. [110] gives $f_{\text{eff}} = 0.25$ (0.33) for μ (b) final states at $m_\chi = 100$ GeV, which we average to $f_{\text{eff}} = 0.27$ for our benchmark two-mediator model with 80% $\mu + 20\%$ b final states, to give $\langle \sigma v \rangle < 1.5 \times 10^{-25} (m_\chi/100 \text{ GeV}) \text{cm}^3/\text{s}$. This is plotted on fig. 9 (short dash-dotted curve). It is a somewhat weaker constraint than the latest (Pass 8) limit from Fermi dwarf galaxy observations, but still excludes the preferred regions for the GeV excess fits to Fermi data with two-mediator models, while remaining marginally compatible with the fits to the CCW data.

9.2. Dark matter elastic self-interactions

Self-interactions of dark matter can be significant in our two-mediator model, from t - and u -channel exchange of the lighter mediator. The viscosity cross section, relevant for effects of DM self-scattering on structure forma-

tion, is³

$$\sigma_v = \int d\Omega (1 - \cos^2 \theta) \frac{d\sigma}{d\Omega} = \frac{2g_1^4 m_\chi^2}{3\pi m_{\phi_1}^4} \quad (19)$$

Taking the typical values $g_1 \sim 0.6$, $m_{\phi_1} = 3$ GeV, $m_\chi = 100$ GeV, indicated by our fits, this leads to a cross section per DM mass of order $\sigma_v/m_\chi \sim 10^{-5}$ b/GeV, far below the bound ~ 0.5 b/GeV from simulations of structure formation including DM self-interactions [114]. However, there is freedom in our model to take m_{ϕ_1} as small as $2m_\mu = 0.2$ GeV, if we adjust α_1 to somewhat smaller values ~ 0.01 to compensate for the increased boost from Sommerfeld enhancement in the galactic center.

The self-interaction cross section in such models can have nonperturbative enhancements in analogy to the Sommerfeld effect, which have been studied in detail in ref. [115, 116]. For $\alpha_1 = 0.01$, the latter reference finds that σ_v/m_χ is at the right level to address problems of collisionless cold dark matter for predicting the observed galactic small scale structure, if $m_\chi \cong 165 m_{\phi_1}$ in the region $m_{\phi_1} = 0.2 - 2$ GeV, which overlaps with values needed for explaining the GC excess. These problems include the difficulty for collisionless cold dark matter to correctly predict abundances and maximum masses of dwarf satellite galaxies, as well as the cusp versus core issue for dwarf galaxy DM density profiles; see ref. [117] for a review.

10. COLLIDER CONSTRAINTS

We also consider the collider limits on the particle physics model described in section 6. In a model having additional scalars, which mix with the SM Higgs, one would expect possible limits resulting from the recent observation and measured signals of the Higgs boson at the LHC. Although we find the limits posed by direct detection and relic density results to be more constraining, we include here the collider considerations for completeness.

For the following analysis, we do not initially assume a small mixing angle approximation. We supplement the SM Higgs potential with two real, scalar, singlet fields. Both fields acquire vevs, thereby inducing mixing with the Higgs. The relevant parameters are then the masses of the three scalars, $m_h, m_{\phi_1}, m_{\phi_2}$, and the two mixing angles, θ_{1h}, θ_{2h} . Mixing between the field and mass eigenstates is given according to

³ for scattering of identical particles, this is more appropriate than weighting by $(1 - \cos \theta)$ since it treats scattering by 180° as equivalent to forward scattering

$$\begin{pmatrix} \tilde{h} \\ \tilde{\phi}_1 \\ \tilde{\phi}_2 \end{pmatrix} = \begin{pmatrix} c_{\theta_{1h}} c_{\theta_{2h}} & s_{\theta_{1h}} & c_{\theta_{1h}} s_{\theta_{2h}} \\ -s_{\theta_{1h}} c_{\theta_{2h}} & c_{\theta_{1h}} & -s_{\theta_{1h}} s_{\theta_{2h}} \\ -s_{\theta_{2h}} & 0 & c_{\theta_{2h}} \end{pmatrix} \begin{pmatrix} h \\ \phi_1 \\ \phi_2 \end{pmatrix} \quad (20)$$

where (c, s) denote (\cos, \sin) , respectively.

The scalar couplings to standard model particles are then simply the SM Higgs couplings, scaled by $c_{\theta_{1h}} c_{\theta_{2h}}$, $s_{\theta_{1h}}$, $c_{\theta_{1h}} s_{\theta_{2h}}$, for h , ϕ_1 , and ϕ_2 respectively. We take h to be the recently discovered Higgs boson, setting $m_h = 125.6$ GeV, and take ϕ_1 to be the lighter scalar, such that $m_{\phi_1} < m_{\phi_2}$. We determine the allowed values of the two mixing angles, using the publicly available code HiggsBounds 4.2.0 [118–121] and HiggsSignals 1.3.0 [122, 123]. We fix the values of the masses, such that m_h agrees with the discovered Higgs, as discussed above, and the values of m_{ϕ_i} are those preferred by fits to the GC excess,

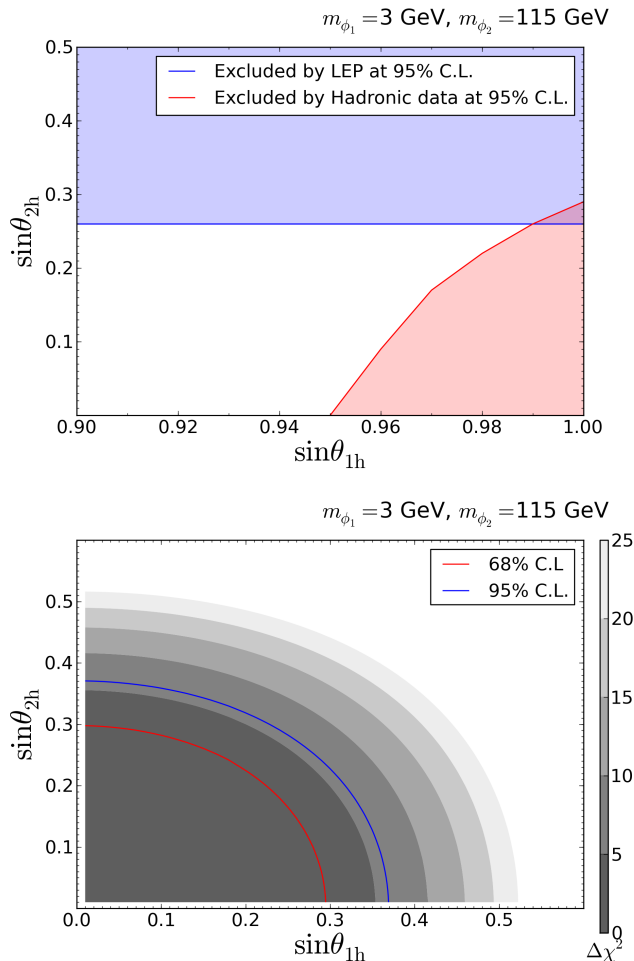


Figure 13: Excluded regions of $(\theta_{1h}, \theta_{2h})$ parameter space, under collider constraints. Top: blue (red) shaded region is excluded at 95% c.l. by LEP (LHC/Tevatron) exclusion limits. Bottom: preferred regions, compatible with LHC Higgs signal strength measurements. Red and blue curves correspond to 68% and 95% c.l.

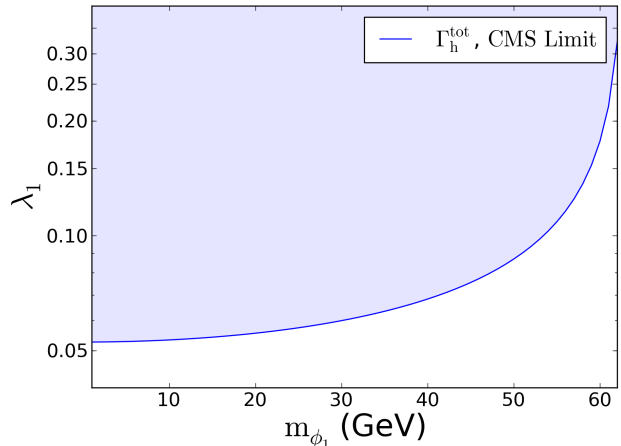


Figure 14: Upper limit on ϕ_1 -Higgs cross coupling vs. m_{ϕ_1} , from CMS constraint on the total Higgs width, at 95% c.l. The shaded region is excluded.

$m_{\phi_1} = 3$ GeV and $m_{\phi_2} = 115$ GeV.

The result is shown in fig. 13. The upper figure shows the regions excluded by LEP and hadronic (Tevatron and LHC) exclusion Higgs searches, obtained by HiggsBounds, while the lower one shows the regions preferred by compatibility with the observed Higgs signal strengths. The set of experimental results and specific Higgs channels that we use for the Higgs signal limit, can be found in refs [124–133]. For a complete list of the results used in the exclusion bounds analysis, see [121] and references therein.

In the described analysis of Higgs signal limits, we only consider the effect of the mixing angles on scaling of the scalar couplings. In principle, new contributions to the width may further suppress the branching ratio, and signal rate, in some channels. For simplicity, we present the results taking only SM decays of the scalars, as the collider limits turn out to be much less constraining than other limits considered here.

For the mass hierarchy that is suggested by the GC considerations, one must also consider the additional contributions to the Higgs width, arising from decays to the light scalar, $h \rightarrow \phi_1 \phi_1$. Returning to the small mixing approximation, the new contribution to the width is given by

$$\Gamma_{h \rightarrow \phi_1 \phi_1} = \frac{\lambda_1^2 \nu^2}{32\pi m_h} \left(1 - \frac{4m_{\phi_1}^2}{m_h^2} \right)^{1/2} \quad (21)$$

A recent CMS analysis [134] presents an upper limit on the Higgs total width, obtained from the ratio of measurements of off-shell and on-shell Higgs production and decay in the $H \rightarrow ZZ$ channel. CMS finds $\Gamma_h < 4.2 \Gamma_h^{SM}$, with $\Gamma_h^{SM} = 4.15$ MeV. We find the upper limit on the cross coupling shown in fig. 14.

11. CONCLUSIONS

In this study we compared two new data sets,⁴ characterizing the excess gamma rays from the galactic center, to predictions from models where dark matter annihilates into light mediators that subsequently decay into standard model particles. In contrast to models with direct annihilation into heavy quarks, these are more easily compatible with direct detection and cosmic ray antiproton constraints, as we have demonstrated. In a first approach, general admixtures of final state particles yielded good fits, revealing a preference for the data to be described by decays mostly to muons (electrons being excluded by AMS-02 data) and b quarks, with dark matter masses in the range 40 – 140 GeV. Either Majorana or Dirac dark matter are viable possibilities.

We then argued that this might be more naturally accomplished with two scalar mediators ϕ_i mixing with the Higgs, such that ϕ_1 decays primarily to $\mu^+\mu^-$ and $\phi_2 \rightarrow bb$, as a consequence of the mediator masses. Encouragingly, fits to the data in this two-mediator model were consistent with masses in the desired ranges $2m_\mu < m_{\phi_1} < 2m_\tau$, $2m_b < m_{\phi_2} < m_\chi$. Moreover quite reasonable perturbative values of the mediator couplings to χ give consistent results. To avoid p -wave suppression of the annihilation cross section we invoked parity violating couplings, which turn out to be somewhat smaller than the parity-conserving ones.

An interesting feature of these models is that the best-fit cross sections for annihilation in the galactic center are several times larger than the value needed for achieving the right thermal relic density. We showed that this can be consistent due to Sommerfeld enhanced annihilation in the galaxy, due to multiple exchanges of the lighter of the two mediators, taking $m_{\phi_1} = 3$ GeV as a benchmark model. It only requires that the scalar coupling of ϕ_1 to χ be of order $g_1 \sim 0.5$. If the light mediator mass is somewhat lower, the cross section for elastic DM self-scattering can have the right magnitude for addressing the missing satellite and cusp-core problems from simulations of structure formation. Improved CMB constraints anticipated from Planck data may be in tension with the best fit regions of parameter space.

LHC constraints on the couplings and mixing angles of the mediators are relatively weak compared to those from direct detection. The latter provides good prospects for independent confirmation of our model, requiring that the cross-coupling between ϕ_1 and the Higgs boson be $\lesssim 10^{-3}$. No fine tuning in the technical sense is needed to satisfy this constraint, but neither is there any symmetry reason for the coupling to be small.

The allowed parameter space in $\langle\sigma v\rangle$ versus m_χ shows some tension with the latest Fermi-LAT constraints on dark matter annihilation in dwarf spheroidals, especially for the fit to the Fermi GeV excess data. Planck constraints on distortions to the CMB are in tension at a similar level. The fit to the CCW excess is also challenged by these results, though to a lesser extent. More optimistically, as we were completing this work, preliminary evidence for a positive signal from the dwarf galaxy Reticulum II appeared [135], at a level consistent with expectations from the GC excess.

Acknowledgments. We thank S. Murgia for helpful correspondence about the Fermi GeV excess spectrum, and M. Reece for stimulating discussions. J.C. is supported by the Natural Sciences and Engineering Research Council (NSERC) of Canada. The work of Z.L. is supported by the Tsinghua University Funds (under Grant No. 543481001 and Grant No. 523081007).

E_γ [GeV]	$d\Phi/dE_\gamma d\Omega$	σ_{stat}	σ_{sys}
1.122	1.587e-06	1.036e-07	8.225e-07
1.413	1.624e-06	7.138e-08	5.810e-07
1.778	1.483e-06	5.330e-08	3.240e-07
2.239	1.122e-06	4.272e-08	1.226e-07
2.818	7.298e-07	3.655e-08	5.857e-08
3.548	4.265e-07	3.106e-08	4.964e-08
4.467	2.475e-07	2.074e-08	3.511e-08
5.623	1.405e-07	1.270e-08	2.735e-08
7.079	7.662e-08	8.267e-09	1.874e-08
8.913	4.039e-08	5.435e-09	1.226e-08
11.220	2.272e-08	3.688e-09	7.959e-09
14.125	1.345e-08	2.433e-09	4.936e-09
17.783	7.828e-09	1.566e-09	3.016e-09
22.387	4.341e-09	1.023e-09	1.820e-09
28.184	2.503e-09	6.953e-10	1.115e-09
35.481	1.600e-09	4.805e-10	6.589e-10
44.668	1.029e-09	3.146e-10	4.090e-10
56.234	5.832e-10	2.113e-10	2.782e-10
70.795	2.753e-10	1.355e-10	1.556e-10
89.125	9.287e-11	7.851e-11	6.110e-11

Table III: Energy flux derived from Fermi collaboration’s presentation [83] for the galactic center gamma ray excess, and statistical along with systematic errors as described in section 3.2. The flux intensity is obtained by averaging the observed total flux over the $15^\circ \times 15^\circ$ square around the GC. Flux units are $\text{GeV}^{-1}\text{cm}^{-2}\text{s}^{-1}\text{sr}^{-1}$.

⁴ in particular, the Fermi collaboration spectrum determined within energy bands, as opposed to their ansatz using a power law with exponential cutoff, has not previously been analyzed with respect to dark matter models

Appendix A: Fermi Spectrum

We list the Fermi spectrum in table III.

Appendix B: Spectrum from decay to muons

For completeness, we present the photon spectrum from $\phi \rightarrow \mu^+ \mu^-$ in the rest frame of ϕ [79, 87]. It includes photons from final state radiation and from radiative decays. Final state radiation gives the contribution

$$\frac{dN_{FSR}}{dx} = \frac{\alpha_{em}}{\pi} \frac{1 + (1-x)^2}{x} \left[-1 + \ln \left(\frac{m_\phi^2(1-x)}{m_\mu^2} \right) \right], \quad (\text{B1})$$

where $x = 2E_\gamma/m_\phi$. The contribution from radiative decay is

$$\begin{aligned} \frac{dN_{rad}}{dx} = & \frac{\alpha_{em}}{3\pi x} \left\{ -\frac{17}{2} - \frac{3}{2}x + \frac{191}{12}x^2 - \frac{23}{3}x^3 + \frac{7}{4}x^4 \right. \\ & + \left(3 + \frac{2}{3}x - 6x^2 + 3x^3 - \frac{2}{3}x^4 + 5x \ln x \right) \ln \frac{1}{r} \\ & + \left(3 + \frac{2}{3}x - 6x^2 + 3x^3 - \frac{2}{3}x^4 \right) \ln(1-x) \\ & \left. - \frac{28}{3}x \ln x + 5x \ln(1-x) \ln x + 5x \text{Li}_2(1-x) \right\} \quad (\text{B2}) \end{aligned}$$

where $r = \frac{m_\phi^2}{m_\mu^2} \ll 1$, and the range of x is $(0, 1)$ which does not depend on r since r is negligible. The sum of (B1) and (B2) gives us the total photon spectrum from annihilation to muons.

Appendix C: Determination of couplings

Here we show how the couplings of the mediators to dark matter are analytically determined from the various observational constraints. We parametrize the annihilation cross section as

$$\langle \sigma v \rangle = ax + by + cF^2 \quad (\text{C1})$$

where $x = (g_1 g_{1,5})^2$, $y = (g_2 g_{2,5})^2$, and a, b, c are the functions of m_χ, m_{ϕ_2} in (13). The ratio R of muons to

quarks resulting from the annihilations is

$$R = \frac{ax + cF^2/2}{by + cF^2/2} \quad (\text{C2})$$

Setting the cross section equal to the relic density value $\langle \sigma v \rangle_0$ and using (C2), we can solve for x and y , for a given value of F :

$$\begin{aligned} x &= \frac{1}{a} \left(\frac{\langle \sigma v \rangle_0}{1+R^{-1}} - \frac{c}{2} F^2 \right) \\ y &= \frac{1}{b} \left(\frac{\langle \sigma v \rangle_0}{1+R} - \frac{c}{2} F^2 \right) \end{aligned} \quad (\text{C3})$$

Since $x, y \geq 0$, this constrains

$$|F| \leq F_{\max} = \left(\frac{2\langle \sigma v \rangle_0}{c} \right)^{1/2} \min \left[\frac{1}{\sqrt{1+R}}, \sqrt{\frac{R}{1+R}} \right] \quad (\text{C4})$$

The minimum value of α_1 needed for sufficient Sommerfeld enhancement determines $g_1 = \sqrt{4\pi\alpha_1}$; then $g_{1,5} = \sqrt{x}/g_1$ and $g_{2,5} = \sqrt{y}/g_2$, where we should allow for both possible signs of \sqrt{x} and \sqrt{y} . Eliminating $f_{1,5}$ and $f_{2,5}$ in equation (14) for F results in a quadratic equation for $s = g_1/g_2$:

$$s = \frac{F \pm \sqrt{F^2 - 4\sqrt{x}\sqrt{y}(1-q^2)}}{2\sqrt{y}(1+q)} \quad (\text{C5})$$

where $q = m_{\phi_2}^2/4m_\chi^2$. The smallest value of $|s|$ is found when the signs of the two terms in the numerator of (C5) are opposite. We can take $F > 0$ and the lower sign while keeping $s > 0$ if $\sqrt{y} < 0$, corresponding to the choice of all couplings except for $g_{2,5}$ being positive. (Alternatively, we could take all couplings except for $g_{1,5}$ positive and $F < 0$, but there is no physical difference.) One can explore the range of possible couplings by allowing F to vary between 0 and F_{\max} .

-
- [1] D. Hooper and L. Goodenough, Phys. Lett. B **697**, 412 (2011) [arXiv:1010.2752 [hep-ph]].
 - [2] D. Hooper and T. Linden, Phys. Rev. D **84**, 123005 (2011) [arXiv:1110.0006 [astro-ph.HE]].
 - [3] K. N. Abazajian and M. Kaplinghat, Phys. Rev. D **86**, 083511 (2012) [arXiv:1207.6047 [astro-ph.HE]].
 - [4] T. Daylan, D. P. Finkbeiner, D. Hooper, T. Linden, S. K. N. Portillo, N. L. Rodd and T. R. Slatyer, arXiv:1402.6703 [astro-ph.HE].
 - [5] B. Zhou, Y. F. Liang, X. Huang, X. Li, Y. Z. Fan, L. Feng and J. Chang, arXiv:1406.6948 [astro-ph.HE].
 - [6] F. Calore, I. Cholis and C. Weniger, arXiv:1409.0042 [astro-ph.CO].
 - [7] K. N. Abazajian, JCAP **1103**, 010 (2011) [arXiv:1011.4275 [astro-ph.HE]].
 - [8] K. N. Abazajian, N. Canac, S. Horiuchi and M. Kaplinghat, arXiv:1402.4090 [astro-ph.HE].
 - [9] Q. Yuan and B. Zhang, arXiv:1404.2318 [astro-ph.HE].
 - [10] J. Petrović, P. D. Serpico and G. Zaharijas, JCAP **1502**, no. 02, 023 (2015) [arXiv:1411.2980 [astro-ph.HE]].
 - [11] Q. Yuan and K. Ioka, arXiv:1411.4363 [astro-ph.HE].
 - [12] J. Petrovic, P. D. Serpico and G. Zaharijas, JCAP **1410**, no. 10, 052 (2014) [arXiv:1405.7928 [astro-ph.HE]].
 - [13] E. Carlson and S. Profumo, Phys. Rev. D **90**, no. 2, 023015 (2014) [arXiv:1405.7685 [astro-ph.HE]].
 - [14] D. Hooper, I. Cholis, T. Linden, J. Siegal-Gaskins

- and T. Slatyer, Phys. Rev. D **88**, 083009 (2013) [arXiv:1305.0830 [astro-ph.HE]].
- [15] I. Cholis, D. Hooper and T. Linden, arXiv:1407.5625 [astro-ph.HE].
- [16] F. Calore, M. Di Mauro and F. Donato, arXiv:1412.4997 [astro-ph.HE].
- [17] L. A. Anchordoqui and B. J. Vlcek, Phys. Rev. D **88**, 043513 (2013) [arXiv:1305.4625 [hep-ph]].
- [18] N. Okada and O. Seto, Phys. Rev. D **89**, no. 4, 043525 (2014) [arXiv:1310.5991 [hep-ph]].
- [19] W. C. Huang, A. Urbano and W. Xue, JCAP **1404**, 020 (2014) [arXiv:1310.7609 [hep-ph]].
- [20] K. P. Modak, D. Majumdar and S. Rakshit, arXiv:1312.7488 [hep-ph].
- [21] C. Boehm, M. J. Dolan, C. McCabe, M. Spannowsky and C. J. Wallace, JCAP **1405**, 009 (2014) [arXiv:1401.6458 [hep-ph]].
- [22] T. Lacroix, C. Boehm and J. Silk, Phys. Rev. D **90**, no. 4, 043508 (2014) [arXiv:1403.1987 [astro-ph.HE]].
- [23] A. Hektor and L. Marzola, Phys. Rev. D **90**, no. 5, 053007 (2014) [arXiv:1403.3401 [hep-ph]].
- [24] A. Alves, S. Profumo, F. S. Queiroz and W. Shepherd, Phys. Rev. D **90**, no. 11, 115003 (2014) [arXiv:1403.5027 [hep-ph]].
- [25] A. Berlin, D. Hooper and S. D. McDermott, Phys. Rev. D **89**, 115022 (2014) [arXiv:1404.0022 [hep-ph]].
- [26] P. Agrawal, B. Batell, D. Hooper and T. Lin, Phys. Rev. D **90**, 063512 (2014) [arXiv:1404.1373 [hep-ph]].
- [27] E. Izaguirre, G. Krnjaic and B. Shuve, arXiv:1404.2018 [hep-ph].
- [28] D. G. Cerdezo, M. Peir and S. Robles, JCAP **1408**, 005 (2014) [arXiv:1404.2572 [hep-ph]].
- [29] S. Ipek, D. McKeen and A. E. Nelson, Phys. Rev. D **90**, no. 5, 055021 (2014) [arXiv:1404.3716 [hep-ph]].
- [30] P. Ko, W. I. Park and Y. Tang, JCAP **1409**, 013 (2014) [arXiv:1404.5257 [hep-ph]].
- [31] D. K. Ghosh, S. Mondal and I. Saha, JCAP **1502**, no. 02, 035 (2015) [arXiv:1405.0206 [hep-ph]].
- [32] T. Han, Z. Liu and S. Su, JHEP **1408**, 093 (2014) [arXiv:1406.1181 [hep-ph]].
- [33] W. Detmold, M. McCullough and A. Pochinsky, Phys. Rev. D **90**, no. 11, 115013 (2014) [arXiv:1406.2276 [hep-ph]].
- [34] L. Wang and X. F. Han, Phys. Lett. B **739**, 416 (2014) [arXiv:1406.3598 [hep-ph]].
- [35] B. D. Fields, S. L. Shapiro and J. Shelton, Phys. Rev. Lett. **113**, 151302 (2014) [arXiv:1406.4856 [astro-ph.HE]].
- [36] C. Arina, E. Del Nobile and P. Panci, Phys. Rev. Lett. **114**, 011301 (2015) [arXiv:1406.5542 [hep-ph]].
- [37] C. Cheung, M. Papucci, D. Sanford, N. R. Shah and K. M. Zurek, Phys. Rev. D **90**, no. 7, 075011 (2014) [arXiv:1406.6372 [hep-ph]].
- [38] J. Huang, T. Liu, L. T. Wang and F. Yu, Phys. Rev. D **90**, no. 11, 115006 (2014) [arXiv:1407.0038 [hep-ph]].
- [39] C. Balz and T. Li, Phys. Rev. D **90**, no. 5, 055026 (2014) [arXiv:1407.0174 [hep-ph]].
- [40] P. Ko and Y. Tang, JCAP **1501**, 023 (2015) [arXiv:1407.5492 [hep-ph]].
- [41] S. Baek, P. Ko and W. I. Park, arXiv:1407.6588 [hep-ph].
- [42] N. Okada and O. Seto, Phys. Rev. D **90**, no. 8, 083523 (2014) [arXiv:1408.2583 [hep-ph]].
- [43] K. Ghorbani, JCAP **1501**, no. 01, 015 (2015) [arXiv:1408.4929 [hep-ph]].
- [44] N. F. Bell, S. Horiuchi and I. M. Shoemaker, Phys. Rev. D **91**, no. 2, 023505 (2015) [arXiv:1408.5142 [hep-ph]].
- [45] A. D. Banik and D. Majumdar, arXiv:1408.5795 [hep-ph].
- [46] D. Borah and A. Dasgupta, Phys. Lett. B **741**, 103 (2015) [arXiv:1409.1406 [hep-ph]].
- [47] M. Cahill-Rowley, J. Gainer, J. Hewett and T. Rizzo, JHEP **1502**, 057 (2015) [arXiv:1409.1573 [hep-ph]].
- [48] J. H. Yu, Phys. Rev. D **90**, no. 9, 095010 (2014) [arXiv:1409.3227 [hep-ph]].
- [49] J. Guo, J. Li, T. Li and A. G. Williams, arXiv:1409.7864 [hep-ph].
- [50] J. Cao, L. Shang, P. Wu, J. M. Yang and Y. Zhang, arXiv:1410.3239 [hep-ph].
- [51] M. Heikinheimo and C. Spethmann, JHEP **1412**, 084 (2014) [arXiv:1410.4842 [hep-ph]].
- [52] P. Agrawal, B. Batell, P. J. Fox and R. Harnik, arXiv:1411.2592 [hep-ph].
- [53] K. Cheung, W. C. Huang and Y. L. S. Tsai, arXiv:1411.2619 [hep-ph].
- [54] F. Calore, I. Cholis, C. McCabe and C. Weniger, arXiv:1411.4647 [hep-ph].
- [55] A. Biswas, arXiv:1412.1663 [hep-ph]; A. Biswas, D. Majumdar and P. Roy, arXiv:1501.02666 [hep-ph].
- [56] K. Ghorbani and H. Ghorbani, arXiv:1501.00206 [hep-ph].
- [57] D. G. Cerdeno, M. Peiro and S. Robles, arXiv:1501.01296 [hep-ph].
- [58] A. Berlin, A. DiFranzo and D. Hooper, arXiv:1501.03496 [hep-ph].
- [59] C. H. Chen and T. Nomura, arXiv:1501.07413 [hep-ph].
- [60] J. Guo, Z. Kang, P. Ko and Y. Orikasa, arXiv:1502.00508 [hep-ph].
- [61] K. P. Modak and D. Majumdar, arXiv:1502.05682 [hep-ph].
- [62] S. Caron, A. Achterberg, L. Hendriks, R. R. de Austri and C. Weniger, arXiv:1502.05703 [hep-ph].
- [63] A. Berlin, S. Gori, T. Lin and L. T. Wang, arXiv:1502.06000 [hep-ph].
- [64] T. Gherghetta, B. von Harling, A. D. Medina, M. A. Schmidt and T. Trott, arXiv:1502.07173 [hep-ph].
- [65] X. J. Bi, L. Bian, W. Huang, J. Shu and P. F. Yin, arXiv:1503.03749 [hep-ph].
- [66] T. Bringmann, M. Vollmann and C. Weniger, Phys. Rev. D **90**, no. 12, 123001 (2014) [arXiv:1406.6027 [astro-ph.HE]].
- [67] M. Cirelli, D. Gaggero, G. Giesen, M. Taoso and A. Urbano, JCAP **1412** (2014) 12, 045 [arXiv:1407.2173 [hep-ph]].
- [68] D. Hooper, N. Weiner and W. Xue, Phys. Rev. D **86**, 056009 (2012) [arXiv:1206.2929 [hep-ph]].
- [69] C. Boehm, M. J. Dolan and C. McCabe, Phys. Rev. D **90**, no. 2, 023531 (2014) [arXiv:1404.4977 [hep-ph]].
- [70] D. Hooper, T. Linden and P. Mertsch, JCAP **1503**, no. 03, 021 (2015) [arXiv:1410.1527 [astro-ph.HE]].
- [71] M. Abdullah, A. DiFranzo, A. Rajaraman, T. M. P. Tait, P. Tanedo and A. M. Wijangco, arXiv:1404.6528 [hep-ph].
- [72] A. Martin, J. Shelton and J. Unwin, Phys. Rev. D **90**, no. 10, 103513 (2014) [arXiv:1405.0272 [hep-ph]].
- [73] T. Basak and T. Mondal, arXiv:1405.4877 [hep-ph].
- [74] A. Berlin, P. Gratia, D. Hooper and S. D. McDermott, Phys. Rev. D **90**, 015032 (2014) [arXiv:1405.5204 [hep-ph]].

- ph]].
- [75] J. M. Cline, G. Dupuis, Z. Liu and W. Xue, *JHEP* **1408**, 131 (2014) [arXiv:1405.7691 [hep-ph]].
- [76] M. Freytsis, D. J. Robinson and Y. Tsai, *Phys. Rev. D* **91**, no. 3, 035028 (2015) [arXiv:1410.3818 [hep-ph]].
- [77] D. Hooper, arXiv:1411.4079 [hep-ph].
- [78] M. J. Dolan, C. McCabe, F. Kahlhoefer and K. Schmidt-Hoberg, arXiv:1412.5174 [hep-ph].
- [79] J. Liu, N. Weiner and W. Xue, arXiv:1412.1485 [hep-ph].
- [80] G. Elor, N. L. Rodd and T. R. Slatyer, arXiv:1503.01773 [hep-ph].
- [81] A. Rajaraman, J. Smolinsky and P. Tanedo, arXiv:1503.05919 [hep-ph].
- [82] J. Kozaczuk and T. A. W. Martin, arXiv:1501.07275 [hep-ph].
- [83] S. Murgia, presented at Fifth Fermi Symposium, 20-24 Oct. 2014, http://fermi.gsfc.nasa.gov/science/mtgs/symposia/2014/program/08_Murgia.pdf
- [84] M. Aguilar *et al.* [AMS Collaboration], *Phys. Rev. Lett.* **113**, 121102 (2014).
- [85] L. Accardo *et al.* [AMS Collaboration], *Phys. Rev. Lett.* **113**, no. 12, 121101 (2014).
- [86] M. Cirelli, G. Corcella, A. Hektor, G. Hutsi, M. Kadastik, P. Panci, M. Raidal and F. Sala *et al.*, *JCAP* **1103**, 051 (2011) [Erratum-ibid. **1210**, E01 (2012)] [arXiv:1012.4515 [hep-ph], arXiv:1012.4515 [hep-ph]].
- [87] J. Mardon, Y. Nomura, D. Stolarski and J. Thaler, *JCAP* **0905**, 016 (2009) [arXiv:0901.2926 [hep-ph]].
- [88] <https://staff.fnwi.uva.nl/c.weniger/pages/material/>
- [89] L. Bergstrom, T. Bringmann, I. Cholis, D. Hooper and C. Weniger, *Phys. Rev. Lett.* **111**, 171101 (2013) [arXiv:1306.3983 [astro-ph.HE]].
- [90] D. Hooper and W. Xue, *Phys. Rev. Lett.* **110**, no. 4, 041302 (2013) [arXiv:1210.1220 [astro-ph.HE]].
- [91] A. Ibarra, A. S. Lamperstorfer and J. Silk, *Phys. Rev. D* **89**, no. 6, 063539 (2014) [arXiv:1309.2570 [hep-ph]].
- [92] C. Evoli, I. Cholis, D. Grasso, L. Maccione and P. Ullio, *Phys. Rev. D* **85**, 123511 (2012) [arXiv:1108.0664 [astro-ph.HE]].
- [93] A. Urbano and W. Xue, arXiv:1412.3798 [hep-ph].
- [94] S. Orito *et al.* [BESS Collaboration], *Phys. Rev. Lett.* **84**, 1078 (2000) [astro-ph/9906426].
- [95] Y. Asaoka, Y. Shikaze, K. Abe, K. Anraku, M. Fujikawa, H. Fuke, M. Imori and S. Haino *et al.*, *Phys. Rev. Lett.* **88**, 051101 (2002) [astro-ph/0109007].
- [96] M. Boezio *et al.* [WiZard/CAPRICE Collaboration], *Astrophys. J.* **561**, 787 (2001) [astro-ph/0103513].
- [97] O. Adriani, G. A. Bazilevskaia, G. C. Barbarino, R. Bellotti, M. Boezio, E. A. Bogomolov, V. Bonvicini and M. Bongi *et al.*, *JETP Lett.* **96**, 621 (2013) [*Pisma Zh. Eksp. Teor. Fiz.* **96**, 693 (2012)].
- [98] K. Kong and J. C. Park, *Nucl. Phys. B* **888**, 154 (2014) [arXiv:1404.3741 [hep-ph]].
- [99] Feroz, F., Hobson, M. P., Cameron, E., & Pettitt, A. N. 2013, arXiv:1306.2144
- [100] M. Ackermann *et al.* [Fermi-LAT Collaboration], *Phys. Rev. D* **89**, 042001 (2014) [arXiv:1310.0828 [astro-ph.HE]].
- [101] M. Ackermann *et al.* [Fermi-LAT Collaboration], arXiv:1503.02641 [astro-ph.HE].
- [102] Akerib:2013tjd N. Arkani-Hamed, D. P. Finkbeiner, T. R. Slatyer and N. Weiner, *Phys. Rev. D* **79**, 015014 (2009) [arXiv:0810.0713 [hep-ph]].
- [103] S. Cassel, *J. Phys. G* **37**, 105009 (2010) [arXiv:0903.5307 [hep-ph]].
- [104] T. R. Slatyer, *JCAP* **1002**, 028 (2010) [arXiv:0910.5713 [hep-ph]].
- [105] J. M. Cline, K. Kainulainen, P. Scott and C. Weniger, *Phys. Rev. D* **88**, 055025 (2013) [arXiv:1306.4710 [hep-ph]].
- [106] D. S. Akerib *et al.* [LUX Collaboration], *Phys. Rev. Lett.* **112**, 091303 (2014) [arXiv:1310.8214 [astro-ph.CO]].
- [107] X. L. Chen and M. Kamionkowski, *Phys. Rev. D* **70**, 043502 (2004) [astro-ph/0310473].
- [108] D. P. Finkbeiner, S. Galli, T. Lin and T. R. Slatyer, *Phys. Rev. D* **85**, 043522 (2012) [arXiv:1109.6322 [astro-ph.CO]].
- [109] T. R. Slatyer, *Phys. Rev. D* **87**, no. 12, 123513 (2013) [arXiv:1211.0283 [astro-ph.CO]].
- [110] J. M. Cline and P. Scott, *JCAP* **1303**, 044 (2013) [Erratum-ibid. **1305**, E01 (2013)] [arXiv:1301.5908 [astro-ph.CO]].
- [111] R. Diamanti, L. Lopez-Honorez, O. Mena, S. Palomares-Ruiz and A. C. Vincent, *JCAP* **1402**, 017 (2014) [arXiv:1308.2578 [astro-ph.CO]].
- [112] M. S. Madhavacheril, N. Sehgal and T. R. Slatyer, *Phys. Rev. D* **89**, 103508 (2014) [arXiv:1310.3815 [astro-ph.CO]].
- [113] P. A. R. Ade *et al.* [Planck Collaboration], arXiv:1502.01589 [astro-ph.CO].
- [114] J. Zavala, M. Vogelsberger and M. G. Walker, *Monthly Notices of the Royal Astronomical Society: Letters* **431**, L20 (2013) [arXiv:1211.6426 [astro-ph.CO]].
- [115] S. Tulin, H. B. Yu and K. M. Zurek, *Phys. Rev. Lett.* **110**, no. 11, 111301 (2013) [arXiv:1210.0900 [hep-ph]].
- [116] S. Tulin, H. B. Yu and K. M. Zurek, *Phys. Rev. D* **87**, no. 11, 115007 (2013) [arXiv:1302.3898 [hep-ph]].
- [117] D. H. Weinberg, J. S. Bullock, F. Governato, R. K. de Naray and A. H. G. Peter, arXiv:1306.0913 [astro-ph.CO].
- [118] P. Bechtle, O. Brein, S. Heinemeyer, G. Weiglein and K. E. Williams, *Comput. Phys. Commun.* **181**, 138 (2010) [arXiv:0811.4169 [hep-ph]].
- [119] P. Bechtle, O. Brein, S. Heinemeyer, G. Weiglein and K. E. Williams, *Comput. Phys. Commun.* **182**, 2605 (2011) [arXiv:1102.1898 [hep-ph]].
- [120] P. Bechtle, O. Brein, S. Heinemeyer, O. Stal, T. Stefaniak, G. Weiglein and K. Williams, *PoS CHARGED 2012*, 024 (2012) [arXiv:1301.2345 [hep-ph]].
- [121] P. Bechtle, O. Brein, S. Heinemeyer, O. Stl, T. Stefaniak, G. Weiglein and K. E. Williams, *Eur. Phys. J. C* **74**, no. 3, 2693 (2014) [arXiv:1311.0055 [hep-ph]].
- [122] O. Stl and T. Stefaniak, *PoS EPS -HEP2013*, 314 (2013) [arXiv:1310.4039 [hep-ph]].
- [123] P. Bechtle, S. Heinemeyer, O. Stl, T. Stefaniak and G. Weiglein, *Eur. Phys. J. C* **74**, no. 2, 2711 (2014) [arXiv:1305.1933 [hep-ph]].
- [124] G. Aad *et al.* [ATLAS Collaboration], *Phys. Rev. D* **90**, no. 5, 052004 (2014) [arXiv:1406.3827 [hep-ex]].
- [125] G. Aad *et al.* [ATLAS Collaboration], *Phys. Rev. D* **91**, no. 1, 012006 (2015) [arXiv:1408.5191 [hep-ex]].
- [126] G. Aad *et al.* [ATLAS Collaboration], *JHEP* **1501**, 069 (2015) [arXiv:1409.6212 [hep-ex]].
- [127] The ATLAS collaboration, ATLAS-CONF-2014-060, ATLAS-COM-CONF-2014-078.

- [128] The ATLAS collaboration, ATLAS-CONF-2014-061, ATLAS-COM-CONF-2014-080.
- [129] V. Khachatryan *et al.* [CMS Collaboration], Eur. Phys. J. C **74**, no. 10, 3076 (2014) [arXiv:1407.0558 [hep-ex]].
- [130] S. Chatrchyan *et al.* [CMS Collaboration], Nature Phys. **10**, 557 (2014) [arXiv:1401.6527 [hep-ex]].
- [131] S. Chatrchyan *et al.* [CMS Collaboration], JHEP **1401**, 096 (2014) [arXiv:1312.1129 [hep-ex]].
- [132] S. Chatrchyan *et al.* [CMS Collaboration], Phys. Rev. D **89**, no. 9, 092007 (2014) [arXiv:1312.5353 [hep-ex]].
- [133] [CMS Collaboration], CMS-PAS-HIG-13-005.
- [134] [CMS Collaboration], CMS-PAS-HIG-14-002.
- [135] D. Hooper and T. Linden, arXiv:1503.06209 [astro-ph.HE].